Proposed Spin Amplification for Magnetic Sensors Employing Crystal Defects

Marcus Schaffry,[1] Erik M. Gauger,[1,2,*] John J. L. Morton,[1,3] and Simon C. Benjamin[1,2]
[1]Department of Materials, University of Oxford, Parks Road, Oxford OX1 3PH, United Kingdom
[2]Centre for Quantum Technologies, National University of Singapore, 3 Science Drive 2, Singapore 117543
[3]Clarendon Laboratory, University of Oxford, Parks Road, OX1 3PU, United Kingdom
(Received 19 April 2011; published 10 November 2011)

Recently there have been several theoretical and experimental studies of the prospects for magnetic field sensors based on crystal defects, especially nitrogen vacancy (NV) centers in diamond. Such systems could potentially be incorporated into an atomic force microscopy-like apparatus in order to map the magnetic properties of a surface at the single spin level. In this Letter we propose an augmented sensor consisting of an NV center for readout and an "amplifier" spin system that directly senses the local magnetic field. Our calculations show that this hybrid structure has the potential to detect magnetic moments with a sensitivity and spatial resolution far beyond that of a simple NV center, and indeed this may be the physical limit for sensors of this class.

DOI: 10.1103/PhysRevLett.107.207210 PACS numbers: 85.75.Ss, 06.20.F−, 61.72.jn, 76.70.Hb

A key objective for future sensor technologies is the detection of weak magnetic fields at molecular length scales. There are numerous potential applications in materials science, medical science and biology. An ambitious goal would be to detect the field due to single nuclear spins, in order to gain direct information about the structure of a molecular complex deposited on the surface. This would require unprecedented combination of sensitivity and spatial resolution.

Among the most sensitive magnetic field sensing devices are Hall sensors [1], SQUID sensors [2], force sensors [3], and potentially NV centers in diamond [4–8]. Experimental work has progressed rapidly, enabling, e.g., real-time imaging via frequency locking [9] and nanoscale electric field detection [10]. The sensitivity of NV-center-based magnetometers is steadily improving [11], and a field-gradient allows spatial resolution almost approaching the nanometer scale for proximal spins [12]. Very recently, the detection of spins evidently on the nanocrystal surface has been reported [13].

In this Letter, we propose a significant improvement of the NV center sensor by coupling it to an amplifying spin system (see Fig. 1). We show that the improvement in magnetic moment sensitivity can be expected to be of about 3 orders of magnitude; indeed the augmented NV center may have the highest in-principle performance of any such device.

Generally, a natural limit of the sensitivity of a magnetic field sensor is given by the smallest magnetic field b_{CR} that a probe spin can detect and thus resolve within time T (see the supporting material [14]):

$$b_{\mathrm{CR}} = \frac{e^{\gamma(\tau)}\hbar\sqrt{\tau + t_p}}{\sqrt{T}\tau|\mu_{\mathrm{Prb}}|}. \quad (1)$$

Here, the sensing is performed over $T/(\tau + t_p)$ cycles, where each cycle consists of a sensing period τ and a preparation period t_p. Furthermore, $\gamma(\tau)$ is a positive non-decreasing function describing the dephasing of the spin.

Interestingly, this limit does not depend on the actual value of B. However, a naïve intuition is that the proximity of the probe spin and the sample will be an important characteristic of a practicable sensor, since it determines the strength of the measured magnetic field as well as the sensor's spatial resolution. To quantify this intuition, one can ask the question: how long does it take until the sensor spin detects the magnetic moment associated with an electron or a nuclear spin? In the following, we introduce a magnetic moment sensitivity (in units of $\mathrm{T}/\sqrt{\mathrm{Hz}}$) as a

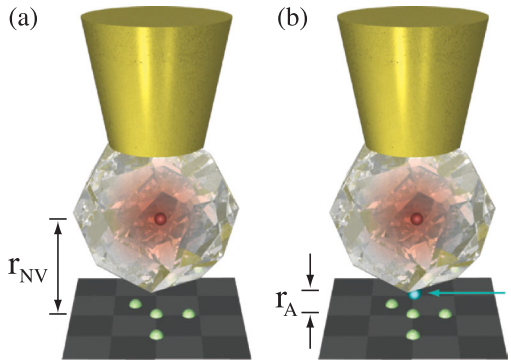

FIG. 1 (color online). (a) Conventional sensor structures: an NV center (red sphere) is embedded in the middle of a diamond nanocrystal that is attached to an AFM-tip (yellow cone). The strength of the magnetic field generated by local spins (green spheres) can be inferred by measuring the NV center through optical means and manipulating it with microwaves. (b) Amplified NV center sensor: the surface of the nanodiamond is decorated with an another spin system (blue sphere) that couples to the NV center inside the diamond. This additional spin system has an amplifying effect and enormously increases the magnetic field sensitivity of the sensor and its spatial resolution.

suitable figure of merit for this question: the magnetic moment sensitivity S of a sensor is given by the number of proton magnetons that can be resolved within the time window $\sqrt{T}$ for a distance r between the probe spin and the sample. The dipole field originating from a proton with magnetic moment μ_p at the position of the probe spin is of order $b = \frac{\mu_0}{4\pi}\frac{2\mu_p}{r^3}$ (where μ_0 is the vacuum permeability), so we obtain

$$S = \frac{\min_\tau(b_{\mathrm{CR}})\sqrt{T}}{b}. \tag{2}$$

We briefly introduce the NV center as a system for field sensing before describing the inherent limitations of this approach and presenting our proposal for improving the characteristics of this class of device. An NV center in diamond possesses spin 1 with the three levels $|0\rangle$ and $|\pm 1\rangle$. The levels $|\pm 1\rangle$ are degenerate in the absence of an external field and shifted from $|0\rangle$ by a zero-field-splitting (ZFS) of about 2.87 GHz. For the purpose of sensing the magnetic field, various two level manifolds can be used, for example $\{|0\rangle, |\pm 1\rangle\}$ or $\{1/\sqrt{2}(|1\rangle + |-1\rangle), (1/\sqrt{2}(|1\rangle - |-1\rangle)\}$ [6].

Figure 2 shows the magnetic moment sensitivity of various classes of sensors. Clearly, NV centers hold the promise of a high field sensitivity combined with a fairly small probe to sample separation. However, in order to further improve the spatial resolution and obtain an even better magnetic moment sensitivity [according to the definition in Eq. (2)] the NV center must be brought even closer to the sample. Because of the cubic dependence of S on r even a modest reduction in the separation leads to a large gain, and for this reason NV centers have been embedded in smaller and smaller nanocrystals [4,5]. However, the size of the diamond crystal surrounding the NV center cannot become arbitrarily small without severely affecting the remarkable coherence time (and thus the sensitivity) of the NV center. In ^{12}C isotopically enriched bulk diamond the room temperature coherence time can be as long as 1.8 ms [15], increasing up to 2.4 ms with dynamic decoupling [16]. On the other hand, the best reported coherence time for a nanodiamond with a diameter of 7 nm is reduced to 1.4 μs [17]. Smaller crystals with a diameter of only 5 nm have been studied in Ref. [18], however the properties of enclosed NV centers are even further degraded in this case. A miniaturization of the crystal hence leads to a reduced field sensitivity in exchange for a smaller separation between the probe and the sample.

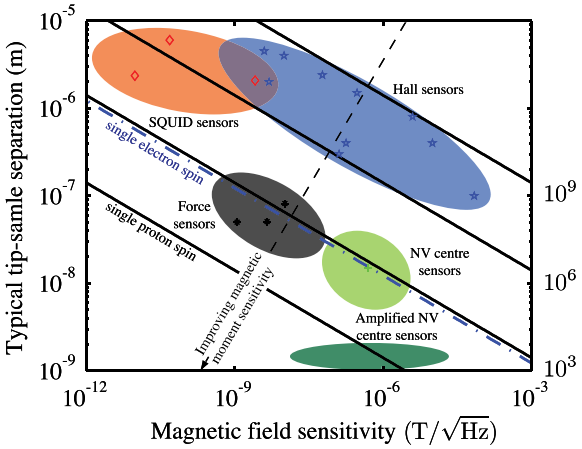

FIG. 2 (color online). Performance of various state-of-the-art and proposed magnetic field sensors (figure adapted from Ref. [33]). The plot shows magnetic sensitivity (per $\sqrt{\mathrm{Hz}}$) (horizontal) versus a typical tip-sample separation. The data points are reported sensitivities from experiments: force sensors [34–36], Hall sensors [37], SQUID sensors [2,38,39], and NV center sensors [4]. The diagonal lines sketch the boundaries for the magnetic moment sensitivity (see Eq. (2)) required to detect 1, 10^3, 10^6, or 10^9 protons (solid black) and a Bohr magneton (blue dash dotted) within 1 s. The potential of our proposed preamplified NV center is illustrated by the dark green ellipse.

We propose to overcome this trade-off situation by bringing the NV center "effectively" closer to the sample without reducing the size of the nanocrystal. This is achieved by attaching an additional spin system on the surface of a nanocrystal which relays the sample magnetic field to the NV center (see Fig. 1). In the simplest implementation, a single electron spin serves as the amplifier. There is a large set of stable $S = 1/2$ organic radicals with coherence times up to 200 μs, which could be attached to the nanocrystal surface [19–22]. Further improvements may be possible by using higher spin systems, e.g., a molecular magnet [23,24]. It may even be possible to make use of more sensitive entangled states with suitably engineered molecular systems [25,26].

For simplicity, we consider an $S = 1/2$ electron spin as the amplifier in the following. The NV center and the amplifier spin are dipole coupled, and we assume the vector connecting the two spins is aligned with the z axis. Both spins experience a (known) homogeneous external magnetic field $\mathbf{B}_0 = (0, 0, B_0)$ and a small magnetic field whose z component B at the position of the amplifier is to be measured. In comparison to the amplifier spin the NV center experiences a weaker sample field cB where the factor $c < 1$ depends on the relative separations. The Hamiltonian thus reads

$$H = -\mu_{\mathrm{NV}}(B_0 + cB)S_{\mathrm{NV},z} + D_{\mathrm{NV}}S_{\mathrm{NV},z}^2 - \mu_A(B_0 + B)S_{A,z} - d(2S_{\mathrm{NV},z}S_{A,z} - S_{\mathrm{NV},x}S_{A,x} - S_{\mathrm{NV},y}S_{A,y}), \tag{3}$$

where $d = \frac{\mu_0}{4\pi}\frac{\gamma_{\mathrm{NV}}\gamma_A\hbar}{\Delta^3}$ is the dipolar coupling constant; γ_{NV} and γ_A are the gyromagnetic ratios of the spins, Δ is the distance between the NV center and the amplifier spin, and D_{NV} denotes the NV center's ZFS constant. Our protocol assumes that the influence of cB on the NV center is much smaller than its coupling to the amplifier spin; this will certainly be justified if the amplifier is an electron spin and the sample field is due to nuclear spins. In addition we

assume that flip-flops between the spins are heavily suppressed and can be neglected, for example, because D_{NV} represents the largest energy in the system, yielding the following effective Hamiltonian

$$H \approx -\mu_{\mathrm{NV}} B_0 S_{\mathrm{NV},z} + D_{\mathrm{NV}} S_{\mathrm{NV},z}^2 - \mu_A (B_0 + B) S_{A,z} - 2d S_{\mathrm{NV},z} S_{A,z}, \quad (4)$$

whose level structure is schematically depicted in Fig. 3.

The field sensing protocol now proceeds as follows. Initially, the system starts in a completely mixed spin state, $\frac{1}{6}\mathbf{1}_6$, so that it needs to be polarized with laser and microwave pulses. As a first step we polarize the NV center by illuminating it with green light, after about 1 μs the NV center will have relaxed to the state $|0\rangle$ with high probability [6], leaving the combined system in the state $|0\rangle\times\langle 0| \otimes \frac{1}{2}\mathbf{1}_2$. Next, we apply a selective microwave π pulse on the transition $|0\rangle|\downarrow\rangle \leftrightarrow |1\rangle|\downarrow\rangle$. For a distance $\Delta =$ 10 nm between the NV center and the amplifier, this transition is split from the neighboring $|0\rangle|\uparrow\rangle \leftrightarrow |1\rangle|\uparrow\rangle$ transition by $2d = 2\frac{\mu_0 g_{\mathrm{NV}} g_A \mu_B^2}{4\pi\Delta^3\hbar} \approx 0.65$ Mrad/s (i.e. 104 kHz). A highly selective π pulse is beneficial for the presently discussed protocol. For this reason we now establish the conditions under which imperfections in the pulse selectivity can be considered negligible. Assuming Lorentzian line broadening of both transitions with a FWHM of $2/T_{2,\mathrm{NV}}$ ($T_{2,\mathrm{NV}}$ is the coherence time of the NV center), a detailed analysis [14] shows that a linewidth overlap of up to 10% meets this requirement and translates into $T_{2,\mathrm{NV}} > 10$ μs. The product of pulse duration and frequency passband $T\times\Delta\omega$ is typically between 2 and 5 [27]. Taking $T = 4/\Delta\omega$ and allowing the passband to overlap with the area of unwanted transition's Lorentzian by at most 5% (allowing us to neglect imperfect pulse selectivity), we thus obtain $\tau_\pi = \frac{4}{2(2d-\cot(0.05\pi)/T_{2,\mathrm{NV}})}$ for the duration of the desired selective π pulse (reducing to $\tau_\pi \approx 1/d$ in the limit of long $T_{2,\mathrm{NV}}$).

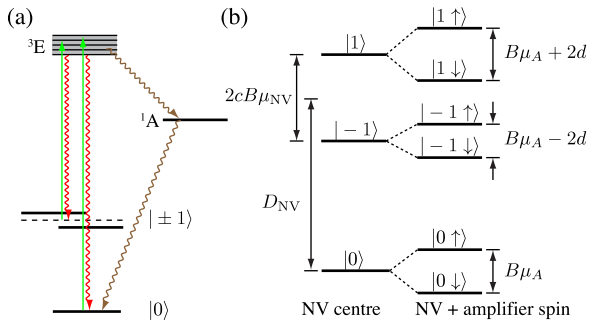

FIG. 3 (color online). (a) Level structure of an NV center. The ground state is a spin triplet with zero field splitting and the excited state has a manifold of levels. Following excitation with green light the dominant decay is spin preserving. However, spin is not always conserved due to an additional decay path to $|0\rangle$ via a metastable state, so that continuous excitation eventually results in a polarised state. (b) Eigenspectrum of H for an amplifier spin $\frac{1}{2}$ system.

Finally, the state of the NV center is measured. There are several ways of performing this measurement. At low temperature the $|0\rangle$ state can be resonantly excited, and hence a single shot readout is possible [28]. However, at room temperature the excitation with a laser can only be done nonresonantly, and therefore the entire triplet ground state is always excited at once. In this case the NV center exhibits spin-dependent photoluminescence, before ultimately being pumped into the $|0\rangle$ state. For the foreseeable future, experiments will only detect a tiny fraction of the emitted photons [6]. Therefore many repetitions may be necessary for conclusive measurements. As each readout cycle pumps the NV center spin into the $|0\rangle$ state we either continuously reiterate the selective π pulse described above after each measurement or employ a nearby nuclear spin analogously to Ref. [29]. In the supplementary material we analyze all three readout possibilities [14] and find similar results in all cases. In this Letter we present the case where the NV center is readout nonresonantly and the selective π pulse is repeatedly applied after each measurement cycle. This leaves the system in one of the well-defined states $|0\rangle|\downarrow\rangle$ or $|0\rangle|\uparrow\rangle$.

Without loss of generality we assume the system is in the state $|0\rangle|\downarrow\rangle$, ready for the magnetic field estimation through several repetitions of the following sensing cycle: A microwave $\frac{\pi}{2}$ pulse creates the superposition $1/\sqrt{2}(|0\downarrow\rangle + |0\uparrow\rangle)$. It is safe to assume that the amplifier spin can be rotated fast and with high fidelity as long as the unknown field corresponds to the smallest energy scale of the system, as can be accomplished with a modest external field. After a sensing time τ, the amplifier spin acquires a relative phase proportional to B. The phase is first mapped onto a population difference between $|0\downarrow\rangle$ and $|0\uparrow\rangle$ with another $\frac{\pi}{2}$ pulse, and then entangled with the NV center spin state with a selective π pulse in the same way as in the initialisation process. The NV center spin state is now read out (also initializing it for the next sensing cycle).

Having described the protocol, we now benchmark the sensitivity improvement of the amplified system over a conventional single NV center sensor. Obviously, the performance of both sensors depends on the decoherence model, which we assume to be fully characterized by $\gamma(t)$. Different forms of $\gamma(t)$ occur corresponding to different predominant dephasing mechanisms, however, typically $\gamma(t)$ can be written as $(t/T_2)^n$ for $n = 1, 2,$ or 3 [6,17].

For our comparison, we consider the levels $|0\rangle$ and $|1\rangle$ of an NV center in the middle of a nanocrystal with radius 10 nm and a control and measurement duration of $t_{p,\mathrm{NV}} \approx 1$ μs per cycle. In contrast, using the electron spin on the surface of the augmented sensor entails an additional control overhead of about τ_π in each measurement cycle, i.e., $t_{p,A} \approx N(t_{p,\mathrm{NV}} + \tau_\pi)$, where N is the number of cycles: $N = \frac{1}{R^2\eta}$ which is given by the measurement

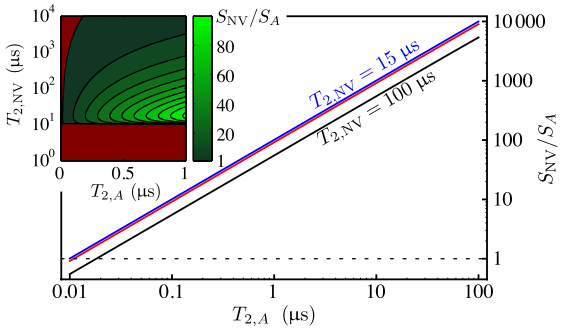

FIG. 4 (color online). Ratio S_{NV}/S_A as a function of the amplifier spin coherence time $T_{2,A}$ for $T_{2,NV} = 100$ μs (black), 30 μs (red), and 15 μs (blue). This ratio gives the factor by which the amplified sensor outperforms a conventional NV center sensor. Here $\gamma(t) = t/T_2$, but we note that the curves for $\gamma(t) = (t/T_2)^{2,3}$ differ approximately only by a prefactor [14]. Other parameters: $r_A = 1$ nm, $r_{NV} = 11$ nm, $\Delta = 10$ nm, $t_{p,NV} = 1$ μs, $t_{p,A} = 1/(R^2\eta)(t_{p,NV} + \tau_\pi)$, $R = 0.2$, $\eta = 0.05$. Inset: excessive line-broadening or a significant mismatch in the coherence times prevent a sensitivity enhancement in the red region (see text).

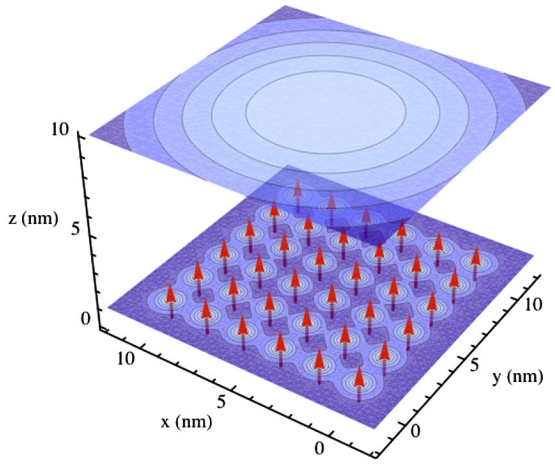

FIG. 5 (color online). The z component of the magnetic field of a regular array of protons calculated in two planes $z = 1$ nm and $z = 10$ nm. The 36 dipoles with the magnetic moment of a proton are placed in the $z = 0$ plane, pointing into the z direction as indicated by the red arrows. The field range of the contour plots spans 43.2 nT in the $z = 10$ nm plane and 2.61 μT for $z = 1$ nm. Individual dipoles are easily resolved at $z = 1$ nm, but at a distance of 10 nm their field looks similar to that of a single stronger magnetic moment. Spatially resolving individual spins at this distance requires a sensitivity that goes far beyond the amount of detail reflected in this plot.

contrast R and the detection efficiency η [30,31]. Figure 4 shows the ratio S_{NV}/S_A with respect to the amplifier coherence time $T_{2,A}$ for several illustrative values of $T_{2,NV}$. The red regions of the inset show the parameter space for which our protocol is not necessarily advantageous, either due to excessive line-broadening preventing a highly selective π pulse on the transition $|0\rangle|\downarrow\rangle \leftrightarrow |1\rangle|\downarrow\rangle$, or because $T_{2,NV}$ is so much larger than $T_{2,A}$ that it more than compensates the benefit of the amplifier spin. Figure 4 impressively demonstrates that the magnetic moment sensitivity can be enhanced by up to 3 orders of magnitude for $T_{2,NV} \approx T_{2,A}$ with realistic parameters. Further improvements may be feasible by substituting the electron spin amplifier with a high spin system or molecular magnet.

We now turn to another important consideration: Given a sensor that can resolve magnetic fields at the level of the single Bohr or even nuclear magneton, its spatial resolution is vitally important for many applications such as mapping the constituent molecules and nuclei of complex organic molecules. Unsurprisingly, it is highly beneficial to be able to move very close to the sample in order to reliably distinguish individual magnetic moments. Figure 5 shows the z component (i.e., the measured component) of the magnetic field for a regular array of protons at two different heights above the surface. If the probe sample separation is of order the distance between individual dipoles, the nuclear spins can be unambiguously resolved (given the required field sensitivity). On the other hand, the field is almost indistinguishable from that of a single stronger dipole if the sensor is scanning at $z = 10$ nm, even with the ability to sense small magnetic fields of order 1 nT.

In summary, we have proposed a practical way of enhancing NV-center-based magnetic field sensor with a preamplifier system. Such an augmented sensor possesses a magnetic moment sensitivity that is capable of resolving individual protons, both in terms of their field strength as well as spatially on an atomic scale. The sensor consists of two essential parts: the NV center for optical readout coupled to a spin-based system for the magnetic field detection in close proximity to the sample. The principal difficulties in implementing our magnetometer are similar to those encountered in earlier NV-center-based designs: the construction of the novel probe tip itself, ideally employing a single defect in a nanocrystal, and achieving the required levels of optical and MW control [4–7]. In addition, our approach involves attaching an amplifier spin to the surface of the crystal. This specific task has not been demonstrated but it is encouraging to note that comparable techniques involving "grabbing" single atoms and molecules are routinely achieved with STM probes, and more recently even with AFM probes at room temperature [32].

We thank Brendon Lovett and Stephanie Simmons for fruitful discussions. This work was supported by the National Research Foundation and Ministry of Education, Singapore, the DAAD (German Academic Exchange Service), the Royal Society, St John's College and Linacre College, Oxford.

*erik.gauger@materials.ox.ac.uk

[1] E. Ramsden, *Hall-Effect Sensors* (Newnes, Oxford, UK, 2006).

[2] M. E. Huber *et al.*, Rev. Sci. Instrum. **79**, 053704 (2008).
[3] M. Poggio and C. L. Degen, Nanotechnology **21**, 342001 (2010).
[4] J. R. Maze *et al.*, Nature (London) **455**, 644 (2008).
[5] G. Balasubramanian *et al.*, Nature (London) **455**, 648 (2008).
[6] J. M. Taylor *et al.*, Nature Phys. **4**, 810 (2008).
[7] C. L. Degen, Appl. Phys. Lett. **92**, 243111 (2008).
[8] N. Zhao *et al.*, Nature Nanotech. **6**, 242 (2011).
[9] R. S. Schoenfeld and W. Harneit, Phys. Rev. Lett. **106**, 030802 (2011).
[10] F. Dolde *et al.*, Nature Phys. **7**, 459 (2011).
[11] P. Maletinsky *et al.*, arXiv:1108.4437.
[12] M. S. Grinolds *et al.*, Nature Phys. **7**, 687 (2011).
[13] B. Grotz *et al.*, New J. Phys. **13**, 055004 (2011).
[14] See Supplemental Material at http://link.aps.org/supplemental/10.1103/PhysRevLett.107.207210 for details on the sensitivity of a single spin and a detailed analysis of measurement strategies for reading out the NV centre spin with respect to the ratio S_{NV}/S_A.
[15] G. Balasubramanian *et al.*, Nature Mater. **8**, 383 (2009).
[16] B. Naydenov *et al.*, Phys. Rev. B **83**, 081201 (2011).
[17] J. Tisler *et al.*, ACS Nano **3**, 1959 (2009).
[18] C. Bradac *et al.*, Nature Nanotech. **5**, 345 (2010).
[19] G. Jeschke and Y. Polyhach, Phys. Chem. Chem. Phys. **9**, 1895 (2007).
[20] M. Lindgren *et al.*, J. Chem. Soc., Perkin Trans. 2 **1997**, No. 12, 2549.
[21] R. Ward *et al.*, J. Magn. Reson. **207**, 164 (2010).
[22] R. M. Brown *et al.*, Phys. Rev. B **82**, 033410 (2010).
[23] M. Mannini *et al.*, Nature (London) **468**, 417 (2010).
[24] G. Christou *et al.*, MRS Bull. **25**, 66 (2000).
[25] J. A. Jones *et al.*, Science **324**, 1166 (2009).
[26] M. Schaffry *et al.*, Phys. Rev. A **82**, 042114 (2010).
[27] M. A. Bernstein, K. F. King, and X. J. Zhou, *Handbook of MRI Pulse Sequences* (Elsevier, New York, 2004).
[28] J. Wrachtrup and F. Jelezko, J. Phys. Condens. Matter **18**, S807 (2006).
[29] P. Neumann *et al.*, Science **329**, 542 (2010).
[30] V. M. Acosta *et al.*, Phys. Rev. B **80**, 115202 (2009).
[31] V. M. Acosta *et al.*, Appl. Phys. Lett. **97**, 174104 (2010).
[32] O. Custance, R. Perez, and S. Morita, Nature Nanotech. **4**, 803 (2009).
[33] C. Degen, Nature Nanotech. **3**, 643 (2008).
[34] D. Rugar *et al.*, Nature (London) **430**, 329 (2004).
[35] C. L. Degen *et al.*, Proc. Natl. Acad. Sci. U.S.A. **106**, 1313 (2009).
[36] H. J. Mamin *et al.*, Nano Lett. **9**, 3020 (2009).
[37] G. Boero *et al.*, Sens. Actuators A, Phys. **106**, 314 (2003).
[38] J. R. Kirtley *et al.*, Appl. Phys. Lett. **66**, 1138 (1995).
[39] B. W. Gardner *et al.*, Rev. Sci. Instrum. **72**, 2361 (2001).